All-silicon tandem solar cells: Practical limits for energy conversion and possible routes for improvement

Xuguang Jia,[1,2,a)] Binesh Puthen-Veettil,[1] Hongze Xia,[1] Terry Chien-Jen Yang,[1] Ziyun Lin,[1] Tian Zhang,[1] Lingfeng Wu,[1] Keita Nomoto,[1] Gavin Conibeer,[1] and Ivan Perez-Wurfl[1]
[1]*School of Photovoltaic and Renewable Energy Engineering, University of New South Wales, Sydney, New South Wales 2052, Australia*
[2]*Jiangsu Collaborative Innovation Center of Photovoltaic Science and Engineering, Changzhou University, Jiangsu, China*

(Received 16 January 2016; accepted 2 June 2016; published online 16 June 2016)

Silicon nanocrystals (Si NCs) embedded in a dielectric matrix is regarded as one of the most promising materials for the third generation photovoltaics, owing to their tunable bandgap that allows fabrication of optimized tandem devices. Previous work has demonstrated fabrication of Si NCs based tandem solar cells by sputter-annealing of thin multi-layers of silicon rich oxide and SiO_2. However, these device efficiencies were much lower than expected given that their theoretical values are much higher. Thus, it is necessary to understand the practical conversion efficiency limits for these devices. In this article, practical efficiency limits of Si NC based double junction tandem cells determined by fundamental material properties such as minority carrier, mobility, and lifetime are investigated. The practical conversion efficiency limits for these devices are significantly different from the reported efficiency limits which use Shockley-Queisser assumptions. Results show that the practical efficiency limit of a double junction cell (1.6 eV Si NC top cell and a 25% efficient c-Si PERL cell as the bottom cell) is 32%. Based on these results suggestions for improvement to the performance of Si nanocrystal based tandem solar cells in terms of the different parameters that were simulated are presented. *Published by AIP Publishing.*
[http://dx.doi.org/10.1063/1.4954003]

I. INTRODUCTION

Realization of a high efficiency solar cell which is also cost-effective is a defining problem in photovoltaics today.[1] One of the major energy losses occurring in solar cells is due to the thermalisation of photo-excited carriers with energy higher than the bandgap of the absorber. This loss single-headedly accounts for an efficiency loss of about 35%.[2] The most practical way to reduce this loss is to subdivide the broad solar spectrum into different energy ranges and to convert each range using a cell with a well-matched bandgap.[3] Spectral filtering like this can be achieved automatically using a tandem solar cell. The tandem solar cell is currently the leading third generation concept which has proven its potential in practice. Efficiencies up to 44.7% at 197× concentration have been achieved with multi-junction tandems made of III–V materials.[4] However, III–V tandem cells do not offer the best solution for market penetration, primarily due to the very high cost of materials and fabrication. Therefore, all-silicon tandem cell presents the most economically viable and environmentally sustainable solution.[5] All-silicon solar cells can be realised using silicon nanocrystals (Si NCs).[3] Due to the quantum confinement effect, reducing the size of the nanocrystal enables the modification of the energy bandgap of the material, in this case, silicon. Si NCs embedded in SiO_2 are employed to obtain the large bandgaps required for the top or intermediate cells in a multi-level tandem cell. Single junction solar cell based on Si NC materials has been developed, and an open circuit voltage of around 500 mV under controlled temperature conditions has been reported.[6–8]

However, the demonstrated efficiencies of such cells were very low, and thus, it is necessary to understand their practical conversion efficiency limits. The Shockley-Queisser (SQ) theoretical maximum efficiency limit of an ideal solar cell is often estimated by the detailed balance model which considers only the bandgap of the absorber; but in a realistic case, the intrinsic properties of the absorber play a key role in the energy conversion process.[9] In this paper, we consider the intrinsic parameters of the absorber, such as the minority carrier mobility, lifetime and series resistance, to calculate the practical efficiency of Si NC based tandem solar cells.

II. FABRICATION OF Si NCs SOLAR CELLS

Various techniques have been developed to synthesize Si NCs, including ion implantation, chemical vapor deposition (CVD), ion beam co-sputtering, and reactive evaporation of silicon rich oxides (SRO).[10–14] Precise control of the growth of nanocrystals to obtain a narrow size distribution has been a challenging problem. Zacharias *et al.* has proposed an effective approach to realize relatively accurate size control by depositing SRO and SiO_2 alternating multilayers, as illustrated in Figure 1.[15]

The Si NC solar cells reported in this work adopt the sputter-anneal fabrication techniques mentioned above.[6,8] A bilayer structure used in these cells consisted of a SiO_2 layer followed by a SRO layer. The multilayer structure consists

a)E-mail: X.jia@outlook.com

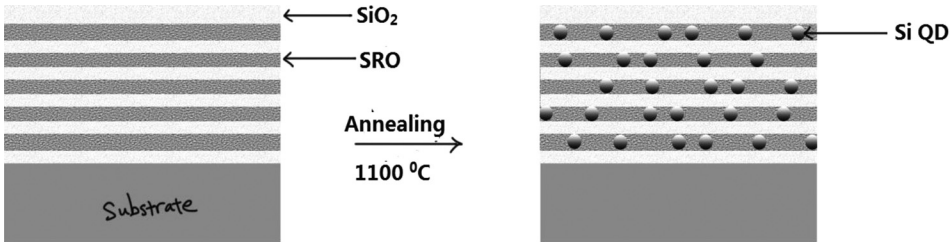

FIG. 1. Schematic diagram of the silicon rich oxide and SiO_2 alternating multilayers (left). Annealing the multilayers at 1100 °C results in the formation of Si nanocrystals which are size-limited to the thickness of the silicon rich oxide layer (right).

of 10 to 50 bilayers annealed in N_2 ambient from 1050 °C to 1150 °C, typically for 1 h. The growth of Si NCs was constrained by the oxide layer and thus the size of NC was limited to the thickness of the SRO layer. This can be confirmed by TEM imaging, as shown in Figure 2. The lattice planes of certain Si NCs in Figure 2(b) can be observed because they are orientated in such a fashion as the electron beam is aligned to the substrate zone axis which in this case is the c-Si (111) plane.[16] A schematic diagram of the Si NC p-i-n device is shown in Figure 3.

III. TANDEM SILICON NANOCRYSTAL BASED SOLAR CELL SIMULATION

A. Tandem cell model with current matching

The energy conversion efficiency of c-Si based tandem cell has been simulated in previous reports.[17,18] However, they only considered all-ideal conditions and did not consider the current matching or the practical conversion efficiency limits of the absorber material.

In the following analysis, a 1-Sun, AM1.5G solar spectrum with an incident light intensity of 1000 W/m^2 is used. The short-circuit current density and the dark saturation current for the top and bottom cells in the tandem are calculated using the photon flux and blackbody radiation, respectively. To find the maximum power point of the device, the *IV* response of the tandem structure is calculated by the following equations:

$$V_{tandem} = V_{top} + V_{bot} = \frac{kT}{q}\left(\ln\left(\frac{J_{SC_{top}} - J_{tandem}}{J_{0_{top}}} + 1\right) + \ln\left(\frac{J_{SC_{bot}} - J_{tandem}}{J_{0_{bot}}} + 1\right)\right), \quad (1)$$

$$P_{tandem} = V_{tandem} \times J_{tandem}, \quad (2)$$

where V_{tandem}, V_{top}, and V_{bot} are the voltages of the tandem, top cell, and bottom cell, respectively, J_{0top} and J_{0bot} are the dark saturation densities of the top and bottom cell, respectively, J_{SCtop} and J_{SCbot} are the short-circuit current densities of the top and bottom cell, respectively, V_{tandem} and J_{tandem} is the voltage and current of the tandem at the maximum power point, and $\frac{kT}{q}$ is the thermal voltage at room temperature.

The maximum power point is found at the point where $\frac{dP_{tandem}}{dV_{tandem}} = 0$.

The efficiency contour diagram for a current-matched double tandem cell is shown in Figure 4. From the figure, the energy bandgap selection range for the top cell is constrained to the top-left region of the bandgap selection for the bottom cell. This is evidently true as the efficiency is non-zero only when the top cell has a larger bandgap compared to the bottom cell. From Figure 4, the maximum efficiency of 45% can be reached by a 1.55 eV top cell fabricated on a 0.96 eV bottom cell. However, if a Si solar cell ($E_g = 1.12$ eV) is used as the bottom cell, the optimum bandgap of the top cell is around 1.60 eV and can achieve an overall efficiency of approximately 43% under ideal conditions.

B. Identification of the practical limits of the technology in terms of the range of bandgaps attainable

1. Efficiency limit beyond SQ assumptions

According to SQ assumptions, all photons with energy above the bandgap are absorbed in the material, and carriers are collected externally for each photon absorbed. To obtain a more practical value for the efficiency limits, the effect of non-radiative processes and finite minority carrier mobility should be considered.

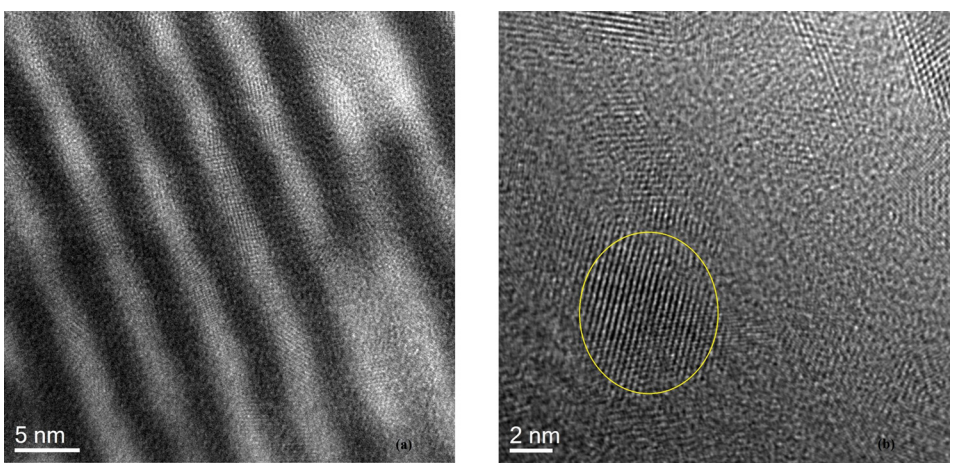

FIG. 2. (a) Energy filtered TEM of SiO_2/SRO multi-layer structure (Si plasmon energy of 17 eV); (b) high resolution TEM (HRTEM) of annealed Si NCs.

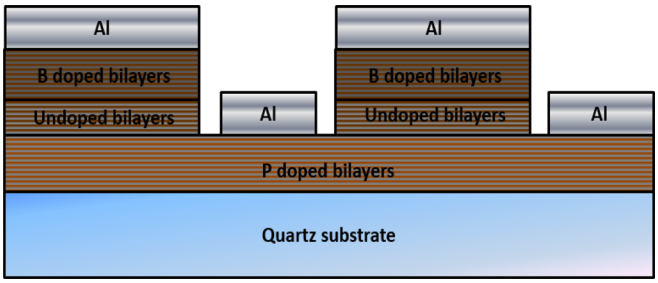

FIG. 3. Schematic diagram of a silicon nanocrystal based p-i-n device.

To simplify the calculations, our model assumes a pn^+ junction solar cell in which the absorption and recombination only occur at the base region. The Si NC layer is modeled as an indirect bandgap semiconductor with bandgap E_g, and absorption coefficient α given by the analytic approximation[19]

$$\alpha(\lambda) = \alpha_0 \left(\frac{E_{ph}(\lambda) - E_g}{kT} \right)^2, \tag{3}$$

where α_0 is the characteristic absorption coefficient of the material, $E_{ph}(\lambda)$ is the incident photon energy at wavelength λ, K is the Boltzmann constant, and T is the cell temperature.

Based on these assumptions, we can obtain the carrier distribution profile by solving the continuity equation in the p region[20]

$$D\frac{d^2n}{dx^2} + G_{int}(x) - \frac{n}{\tau_r} - \frac{n - n_0}{\tau_{nr}} = -G_{sun}(x) - G_{bb}(x). \tag{4}$$

τ_r is radiative minority carrier lifetime, τ_{nr} is the non-radiative minority carrier lifetime, and D is diffusion coefficient. The external generation consist of the equilibrium blackbody generation rate G_{bb}, and non-equilibrium generation rate $G_{sun.}$ $G_{int}(x)$ is the internal generation rate that accounts for photon recycling and is calculated as[20]

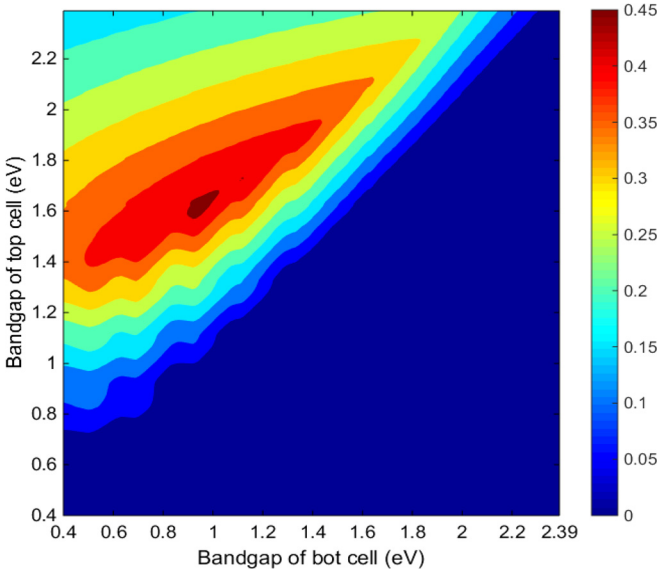

FIG. 4. Efficiency contour plot showing various combinations of top and bottom cell bandgaps for two level tandem devices with current matching.

$$G_{int}(x_g) = \int_{x_r=0}^{x_r=d} \delta G_{int}(x_g, x_r), \tag{5}$$

where

$$\delta G_{int}(x_g, x_r) = \frac{4\pi\bar{n}^2}{h^3c^2} \int_0^\infty \alpha^2 E^2 e^{-\frac{E}{kT}} \cdot f_r(x_g, x_r) dE \frac{n(x_r)}{n_0} \delta x. \tag{6}$$

The boundary conditions of this differential equation are

$$\mathrm{n(x=0)} = n_0 e^{\frac{qV}{kT}},$$

$$\left.\frac{dn}{dx}\right|_{x=d} = \frac{-S_n}{D_n}(n(x=d) - n_0),$$

where d is the thickness of the p region and S_n is the surface recombination velocity. The detailed procedure to solve this linear ordinary differential equation is presented by Mattheis *et al.*[20] Substituting the solution of this equation into the current density equation, one obtains

$$J_n = qD_n \left.\frac{dn}{dx}\right|_{x=0}. \tag{7}$$

The IV relation for an ideal diode under illumination is

$$J = J_{SC} - J_0 \left(exp\left(\frac{qV}{nkT}\right) - 1 \right), \tag{8}$$

where J_{SC} is short circuit current density, J_0 is saturation current density, n is the ideality factor and is assumed to be 1 in the following calculations.

We can extract the short circuit current density, J_{sc}, at $V = 0$ from Eq. (7).

And in the dark conditions

$$J = J_0 \left(exp\left(\frac{qV}{nkT}\right) - 1 \right). \tag{9}$$

J_0 can be extracted at a given voltage.

Since $D_n = \mu_n \frac{kT}{q}$, minority carrier mobility and lifetime can be induced into the efficiency calculation by solving the equations above.

2. Dependence on minority carrier mobility and lifetime

Si NC materials have much lower minority carrier lifetime , τ, and mobility, μ, compared their bulk counterpart.[21] These two limiting factors become the major challenges for improving the performance of Si NC based solar cells. In this section, we theoretically estimate the upper limit of the electron mobility for Si NC material and then investigate the effect of carrier lifetime and mobility on efficiency.

Jiang *et al.* have calculated electron mobility in Si NC super lattice by the effective mass approximation method. Their results show that the electron mobility in this structure is around 1 to 10 $cm^2/V/s$.[22] However, their model is based on the 1D Krönig-Penny model and is over simplistic. In this work, a theoretical model is conducted to simulate the Si-NC

samples using the Linear Combination of Atomic Orbital (LCAO) method implemented in the GPAW codes.[23,24] The reason why the LCAO method was favored over a conventional Density Functional Theorem (DFT) calculation is because the locality of the LCAO method is beneficial in the simulation of large-scale systems like NCs. However, some precision is compromised compared to DFT. Similar to DFT results, the bandgap extracted by this method has an offset, but the curvature of the band is accurate.[23,24] The supercell created is 2.0 nm in diameter containing 433 atoms and 1732 atomic orbitals only, due to the computational limitations. The atomic configuration is illustrated in Figure 5.

After convergence was carefully tested, we adopt the "dzp" basis with the Perdew–Burke–Ernzerhof (PBE) exchange functional and a 2*2*2 k mesh for the self-consistent-field (SCF) calculation. As for the mobility calculation, an even denser k mesh of 8*8*8 is used. The band structure of this Si NC is illustrated in Figure 6.

According to the band structure, the electron mobility is[25]

$$\mu = e\frac{\sum_i \int \tau(i,k)v^2(i,k)\frac{\partial f_{ik}}{\partial \varepsilon_{ik}}dk}{\sum \int f_{ik}dk}, \tag{10}$$

where v is the curvature of the band structure, f is Fermi-Dirac distribution, k is a point in Brillouin zone, i is the band index, and τ is the electron scattering time constant.

To achieve consistency in the calculation, the code was tested on the bulk silicon system and the electron scattering time constant τ_Si was extracted, which was around 1 ps and of the same order of magnitude from literature.[26] The scattering time in Si NCs is around ten times smaller than that of the bulk Si as Si-O bonds create many trap sites that decrease the electron scattering time.[27] By using Eq. (10), the upper limit of the electron mobility in this superlattice structure

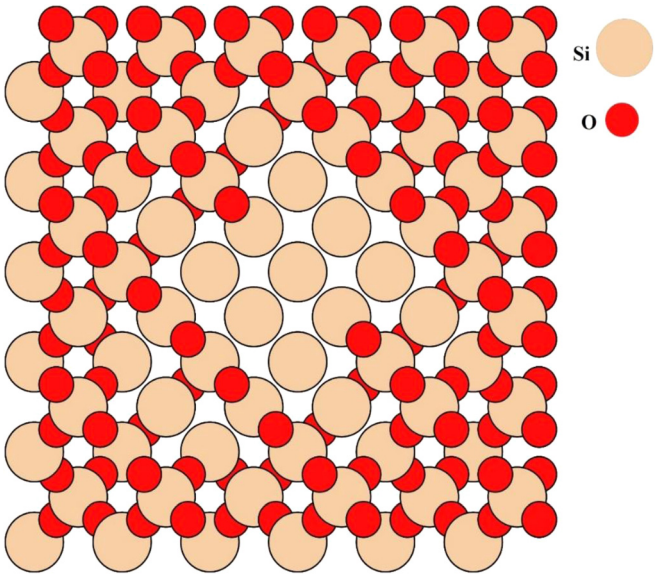

FIG. 5. 2D illustration of atomic configuration for the supper lattice structure.

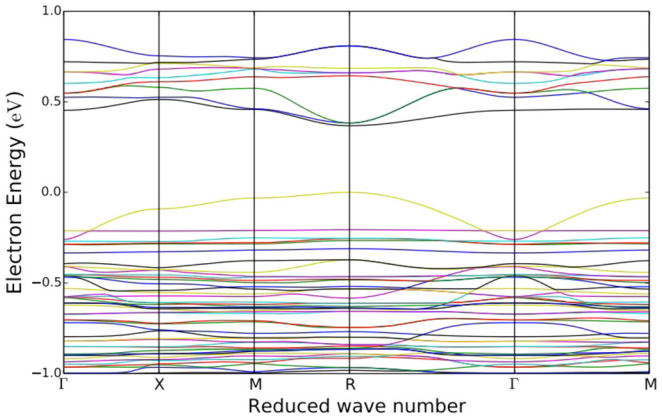

FIG. 6. The band structure diagram of a Si nanocrystal.

can be estimated. Simulation results show that the mobility can reach the order of magnitude of 10^2 cm^2/V/s.

It is known that the minority carrier lifetime τ can be expressed as

$$\frac{1}{\tau} = \frac{1}{\tau_{nr}} + \frac{1}{\tau_r}, \tag{11}$$

where τ_r is radiative lifetime and τ_{nr} is non-radiative lifetime in Eq. (4).

And the radiative recombination rate can be expressed as[28]

$$R_r = R_0\frac{np}{n_i^2}, \tag{12}$$

where R_0 is radiative recombination rate in thermal equilibrium, n, p, and n_i are the electron, hole, and the intrinsic carrier concentration of the material, respectively.

Radiative lifetime can be calculated according to the generalized black body radiation with material refractive index $\tilde{n}$ and absorption coefficient α in thermodynamic equilibrium by[29]

$$\tau_r = \frac{n_0}{R_0} = \frac{n_0}{\frac{2\pi\tilde{n}^2}{h^3c^2}\int_0^\infty \alpha(E)\frac{E^2}{e^{E/kT}-1}dE}, \tag{13}$$

where h is the Planck's constant, c is the light velocity in vacuum, α is the absorption coefficient, and n_0 is the minority carrier concentration for a p type material.

The upper limit of minority carrier lifetime occurs when there is no non-radiative process. Therefore, the upper limit of minority carrier lifetime can be estimated by giving an estimated refractive index of Si NC and an absorption coefficient.

In the following calculations, we modeled the 25% efficient c-Si PERL cell as the bottom cell which has a bandgap of 1.12 eV.[30] The top Si NC based cell is modelled as an n-p+ junction cell with a thickness $d = 300$ nm, which is consistent with the device structures reported previously.[8] The doping concentration of $N_d = 1 \times 10^{17}$ cm^{-3} was used as the optimum value in order to keep the injection level low or medium, so the effect from Auger recombination is negligible.

The surface recombination velocity was assumed to be 0 cm/s to simplify the calculation. The Si NC material still can be regarded as an indirect bandgap semiconductor, but the probability of the non-phonon transitions will increase due to the relaxation of the momentum conservation rule.[19] Thus, here relatively strong absorption coefficients $\alpha(\lambda)$ ($\alpha_0 = 10^2\,\mathrm{cm}^{-1}$) was assumed.[31] $\tilde{n}$ of Si NC was assumed to be 2.2,[32] and according to Eq. (13), the upper limit of minority carrier lifetime in Si NC is around 10^{-5} s.

In the simulations, the minority carrier lifetime was varied from 10^{-9} s to 10^{-4} s and the mobility from 10^{-7} cm^2/V/s to 10^3 cm^2/V/s. The calculated efficiency contour map is shown in Figure 7. From Figure 4, an ideal double tandem with the optimum top cell bandgap of around 1.6 eV under current matching constraints can achieve a maximum efficiency of 43% based on SQ limit assumptions for each cell. But if the upper limit of electron mobility is 10^2 cm^2/V/s, the upper limit of minority carrier lifetime is 10^{-5} s, and the efficiency of the bottom cell is based on practical Si cell (25%) instead of a SQ cell, the efficiency of such a device will degrade to 32% as can be seen from Figure 7.

The contour map can be divided into three regions. In region I, both minority carrier mobility and lifetime are relatively low and the efficiency of the solar cell is close to 0. In region II, the efficiency of the device is sensitive to both minority carrier mobility and lifetime, and an improvement in either lifetime or mobility can dramatically increase the conversion efficiency. An efficiency as high as 20% can be achieved even for materials with mobility of around 1 cm^2/V/s and lifetime over 10 ns. For materials with lower mobility, higher lifetime is required to maintain the same efficiency. However, if the mobility is above 1 cm^2/V/s, the efficiency does not increase as markedly with increasing lifetime as compared to the improvement seen for mobility below 1 cm^2/V/s. This is due to the thinness of the device that limits the benefit of longer diffusion lengths. The reported devices locate on the boundary between region I and region II, and therefore, both minority carrier mobility and lifetime are critical and an improvement of such parameters will bring a breakthrough in the their efficiency.[6] In the region III, the efficiency is mainly determined by the minority carrier mobility and is closed to the theoretical limit.

3. Dependence on series resistance

Series resistance is another important limiting factor in Si NC solar cells. The conductivity of Si NC materials is generally low even in the case of high doping concentrations due to its low mobility. In the case of a thin-film of Si NC material, the sheet resistance can be as high as 1 MΩ/□ and is a detrimental factor for efficiency in lateral device structures.[7] Assuming the upper limit of minority carrier mobility and lifetime, the impact of series resistance on efficiency can be evaluated. After including the area-normalized series resistance R_s (resistance × cell area), the current voltage relation becomes

$$J = J_{SC} - J_0\left[\exp\left(\frac{V - JR_s}{kT}\right) - 1\right]. \tag{14}$$

Series resistance is dependent both on material property and device geometry. For the single junction devices reported by Wu *et al.* and Perez-Wurfl *et al.*, the mesa structure is shown in Figure 8(a). In this structure, series resistance contributions mainly include two parts: vertical resistance R_1 and lateral sheet resistance R_2. According to the device geometry, the current independent series resistance can be estimated by

$$R = R_1 + R_2 = \rho_1\frac{t}{L\cdot d} + R_{sheet}\frac{d}{L} \approx \rho_1\frac{t}{L\cdot d} + \rho_2\frac{d}{L\cdot t}, \tag{15}$$

where t is the thickness of the film, d is the distance between two contacts (20 μm in their report), and L is the length of the metal contact (3.5 mm in their report).

If the resistivity is assumed homogeneous, the ratio of vertical resistance R_1 and lateral resistance R_2 is roughly proportional to $\left(\frac{t}{d}\right)^2$. Generally, the distance d between the two contacts is in the order of micrometer while the thickness of the film is in the order of hundred nanometers. Hence, lateral resistance which is around 100 times larger than vertical resistance is dominant in such device. The sheet resistance in the report is in the order of MΩ/□.[6] Considering the device area of 0.05 cm^2 in their work, the area-normalized R_s is around 250 Ω cm^2, which will dramatically reduce the efficiency to less than 4.7%.

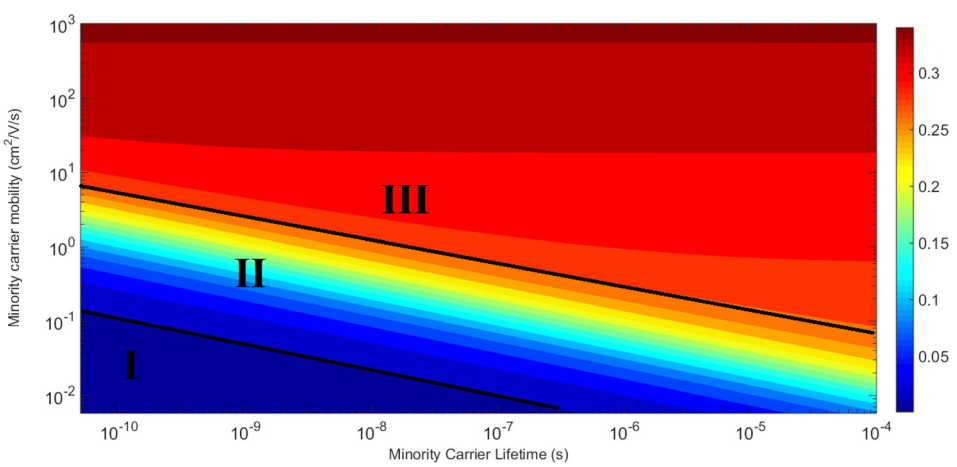

FIG. 7. Efficiency contour plot for the optimized bandgap combination of a two level tandem solar cell. The top cell is a 1.6 eV bandgap Si NC cell, and the bottom cell is a 1.12 eV bandgap silicon solar cell with 25% efficiency.

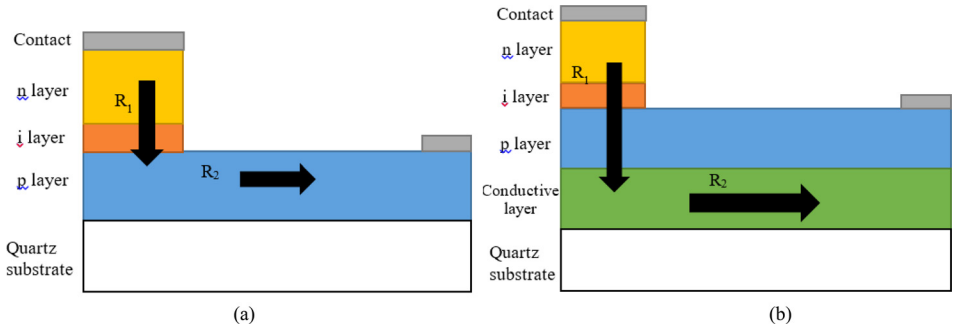

FIG. 8. Schematic diagram of series resistance in Si NC device (a) reported mesa p-i-n structure; (b) p-i-n structure on conductive substrate.

If a conductive substrate can be used as shown in Figure 8(b), the lateral sheet resistance can be down to the order of 100 Ω/□.[33] Thus, the lateral resistance R_2 can be ignored and the vertical resistance R_1 will be dominant in this condition. For the reported devices, R_1 only occupied around 1% of R_s and thus if lateral resistance R_2 was removed, the area-normalized R_s could be reduced from 1–10 Ω cm^2.[34] It can be seen from Figure 9 that the efficiency can reach 30% and the series resistance is no longer a key limiting factor under this condition. Therefore, despite the high resistivity of Si NCs, the vertical device structure using a bottom conductive layer will be able to avoid the large sheet resistance since the thickness of the device is only hundred nanometers. In the double tandem solar cell, it is reasonable to expect such a vertical structure.

C. Possible routes for improving the performance

From the analysis above, it is clear that physical limitations such as low mobility, low carrier lifetime, and high series resistance all need to be tackled if high efficiencies are to be achieved in practice. The following suggests methods to analyze and improve on each of these parameters.

First, the reported minority carrier mobility parameter for Si NC materials is currently in the 0.01 to 1 cm^2/V/s range. As observed from Figure 7, for these values, the theoretical maximum efficiency is still very low for realistic lifetime.[21,35] It is assumed for now, until further evidence is brought forward, that the minority carriers travel through the Si NC material by either tunneling across barriers or hopping from one NC to another or both. Therefore, the mobility can most likely be improved by decreasing the inter-dot separation, improving the uniformity of dot size and decreasing the barrier height.[36] One possible way to achieve this may be by optimizing the Si content in the silicon rich oxide (SRO) layer which improves the uniformity of Si NCs and decreases the inter-dot separation. Another possible way is to replace the SiO_2 layer by other dielectric materials. The application of Si_3N_4 and SiC matrices have been investigated for their relative low barrier height and have some promising results, but further research in this area is still required.[37,38]

Similarly, the minority carrier lifetime of Si NC material can and needs to be improved. A possible way is to decrease the non-radiative recombination since the radiative recombination rate depends on bandgap and absorption coefficient. Presently, it is believed that the dopant concentration used in Si NC materials are much higher than the optimum which causes significant Auger and Shockley-Read-Hall recombinations.[6,39] This is because when research in this area first began, very high doping concentrations were used to make

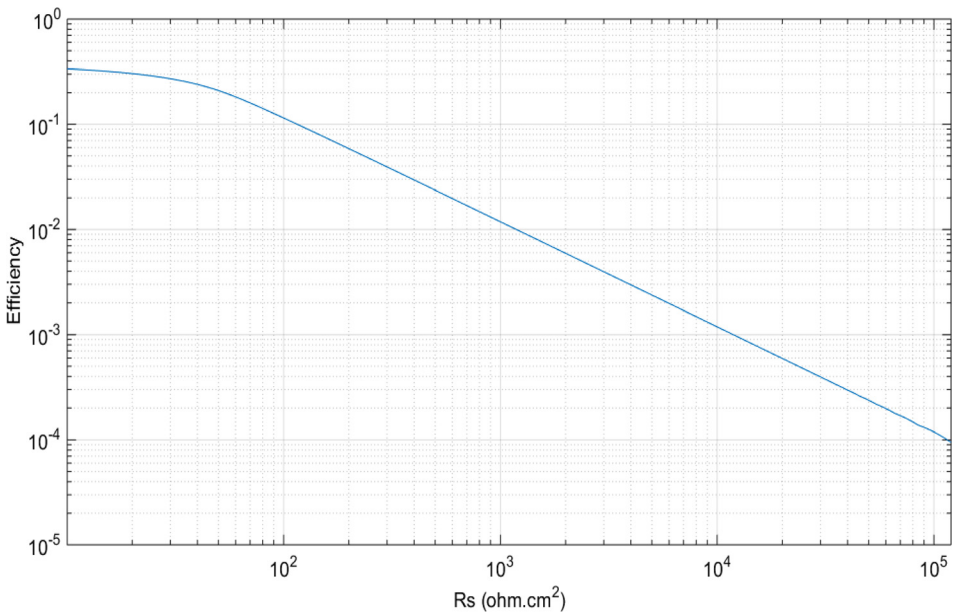

FIG. 9. Impact of area-normalized series resistance in the top cell on a double tandem Si NC solar cell.

the effect of doping more obvious and to make sure that definitive n- and p-type materials were obtained.[40,41] Optimal doping of the NC will decrease the non-radiative recombination, thereby increasing the minority carrier lifetime. Defects due to dangling bonds at the interface between Si NC and SiO_2 interface is another reason for the low effective minority carrier lifetime. Using forming gas (hydrogen and argon mixture) during the deposition or annealing may help with passivating some of the dangling bonds of the Si NC surfaces. Further research in this area should help to improve the performance of Si NC materials in the future.

In terms of series resistance, R_s, results show that the high series resistance of the currently reported device which used non-conductive is mainly caused by the lateral sheet resistance of the Si NCs. To remove this high lateral sheet resistance, an effective way is to apply conductive substrates such as molybdenum, or a transparent conducting oxide.[42,43] If the structure is redesigned to allow vertical current flow through the cell on a transparent conducting substrate, much lower series resistance can be reached since the thickness of such a thin film cell is only a few hundred nanometers. However, the high temperature processing required for nucleating Si NCs has restricted many simple means of growing Si NC thin film on such conductive substrates. A possibility is to use a laser to locally anneal the films, which may allow the use of a large variety of conductive substrates or transparent conducting oxides.[44]

IV. CONCLUSION

This article estimated the practical efficiency limit of double junction tandem solar cells based on the properties of Si NC materials rather than simple SQ assumptions. The simulation results showed that the practical energy conversion efficiency limit of such a double junction Si NC tandem cell is approximately 32%. However, the fabricated devices so far still have extremely low efficiency. The influence of minority carrier mobility, lifetime and series resistance on the practical efficiency of the Si NC tandem solar cell has also been investigated. The simulation quantified the effects of these parameters on the device efficiency and obtained the reasons for the low efficiencies in the present Si NC tandem devices. Based on these observations, suggestions for obtaining higher efficiencies are presented.

ACKNOWLEDGMENTS

This Program has been supported by the Australian Government through the Australian Renewable Energy Agency (ARENA). The Australian Government, through ARENA, is supporting Australian research and development in solar photovoltaic and solar thermal technologies to help solar power become cost competitive with other energy sources. The views expressed herein are not necessarily the views of the Australian Government, and the Australian Government does not accept responsibility for any information or advice contained herein.

[1]M. Green, Sol. Energy **76**(1–3), 3–8 (2004).
[2]G. Conibeer, Mater. Today **10**(11), 42–50 (2007).
[3]G. Conibeer, M. Green, R. Corkish, Y. Cho, E.-C. Cho, C.-W. Jiang, T. Fangsuwannarak, E. Pink, Y. Huang, T. Puzzer, T. Trupke, B. Richards, A. Shalav, and K.-L. Lin, Thin Solid Films **511–512**, 654–662 (2006).
[4]F. Dimroth, M. Grave, P. Beutel, U. Fiedeler, C. Karcher, T. N. D. Tibbits, E. Oliva, G. Siefer, M. Schachtner, A. Wekkeli, A. W. Bett, R. Krause, M. Piccin, N. Blanc, C. Drazek, E. Guiot, B. Ghyselen, T. Salvetat, A. Tauzin, T. Signamarcheix, A. Dobrich, T. Hannappel, and K. Schwarzburg, Prog. Photovoltaics: Res. Appl. **22**(3), 277–282 (2014).
[5]M. A. Green, Prog. Photovoltaics: Res. Appl. **9**(2), 123–135 (2001).
[6]L. Wu, T. Zhang, Z. Lin, X. Jia, B. Puthen-Veettil, T. Chien-Jen Yang, H. Xia, G. Conibeer, and I. Perez-Wurfl, Sol. Energy Mater. Sol. Cells **128**, 435–440 (2014).
[7]G. Conibeer, M. A. Green, D. König, I. Perez-Wurfl, S. Huang, X. Hao, D. Di, L. Shi, S. Shrestha, B. Puthen-Veetil, Y. So, B. Zhang, and Z. Wan, Prog. Photovoltaics: Res. Appl. **19**(7), 813–824 (2011).
[8]I. Perez-Wurfl, X. Hao, A. Gentle, D.-H. Kim, G. Conibeer, and M. A. Green, Appl. Phys. Lett. **95**(15), 153506 (2009).
[9]W. Shockley and H. J. Queisser, J. Appl. Phys. **32**(3), 510–519 (1961).
[10]W. S. Cheong, N. M. Hwang, and D. Y. Yoon, J. Cryst. Growth **204**(1–2), 52–61 (1999).
[11]L. He, T. Inokuma, Y. Kurata, and S. Hasegawa, J. Non-Cryst. Solids **185**(3), 249–261 (1995).
[12]S. Charvet, R. Madelon, R. Rizk, B. Garrido, O. González-Varona, M. López, A. Pérez-Rodríguez, and J. R. Morante, J. Lumin. **80**(1–4), 241–245 (1998).
[13]H. Seifarth, R. Grötzschel, A. Markwitz, W. Matz, P. Nitzsche, and L. Rebohle, Thin Solid Films **330**(2), 202–205 (1998).
[14]S. Chan and P. M. Fauchet, Appl. Phys. Lett. **75**(2), 274–276 (1999).
[15]M. Zacharias, J. Heitmann, R. Scholz, U. Kahler, M. Schmidt, and J. Bläsing, Appl. Phys. Lett. **80**(4), 661–663 (2002).
[16]T. C.-J. Yang, Y. Kauffmann, L. Wu, Z. Lin, X. Jia, B. Puthen-Veettil, T. Zhang, G. Conibeer, I. Perez-Wurfl, and A. Rothschild, Appl. Phys. Lett. **105**(5), 053116 (2014).
[17]T. P. White, N. N. Lal, and K. R. Catchpole, IEEE J. Photovoltaics **4**(1), 208–214 (2014).
[18]F. Meillaud, A. Shah, C. Droz, E. Vallatsauvain, and C. Miazza, Sol. Energy Mater. Sol. Cells **90**(18–19), 2952–2959 (2006).
[19]D. Kovalev, H. Heckler, G. Polisski, and F. Koch, Phys. Status Solidi B **215**(2), 871–932 (1999).
[20]J. Mattheis, J. H. Werner, and U. Rau, Phys. Rev. B **77**(8), 085203 (2008).
[21]D. Lin, L. Ma, G. Conibeer, and I. Perez-Wurfl, Phys. Status Solidi B **248**(2), 472–476 (2011).
[22]C.-W. Jiang and M. A. Green, J. Appl. Phys. **99**(11), 114902 (2006).
[23]A. H. Larsen, M. Vanin, J. J. Mortensen, K. S. Thygesen, and K. W. Jacobsen, Phys. Rev. B **80**(19), 195112 (2009).
[24]J. J. Mortensen, L. B. Hansen, and K. W. Jacobsen, Phys. Rev. B **71**(3), 035109 (2005).
[25]J. Xi, D. Wang, Y. Yi, and Z. Shuai, J. Chem. Phys. **141**(3), 034704 (2014).
[26]S. S. Li, *Semiconductor Physical Electronics* (Springer, USA, 2012).
[27]C.-W. Jiang, Ph.D. thesis, University of New South Wales, 2005.
[28]S. M. Sze and K. K. Ng, *Physics of Semiconductor Devices* (Wiley-Interscience, 2007).
[29]P. Wurfel, J. Phys. C: Solid State Phys. **15**(18), 3967 (1982).
[30]M. A. Green, K. Emery, Y. Hishikawa, W. Warta, and E. D. Dunlop, Prog. Photovoltaics: Res. Appl. **22**(7), 701–710 (2014).
[31]D. Di, H. Xu, I. Perez-Wurfl, M. Green, and G. Conibeer, Nanoscale Res. Lett. **6**, 612 (2011).
[32]X. Jia, L. Wu, Z. Lin, T. Zhang, T. C.-J. Yang, H. Xia, B. Puthen-Veettil, G. Conibeer, and I. Perez-Wurfl, Phys. Status Solidi C **12**(3), 271–274 (2015).
[33]A. K. Kulkarni, K. H. Schulz, T. S. Lim, and M. Khan, Thin Solid Films **345**(2), 273–277 (1999).
[34]S. Yamada, Y. Kurokawa, S. Miyajima, A. Yamada, and M. Konagai, paper presented at the 35th IEEE Photovoltaic Specialists Conference (PVSC), 2010.
[35]M. A. Green, Prog. Photovoltaics: Res. Appl. **20**(4), 472–476 (2012).
[36]B. Puthen-Veettil, R. Patterson, D. König, G. Conibeer, and M. A. Green, J. Appl. Phys. **116**(16), 163707 (2014).
[37]D. Di, H. Xu, I. Perez-Wurfl, M. A. Green, and G. Conibeer, Prog. Photovoltaics: Res. Appl. **19**, 813–824 (2011).

[38]Q. Cheng, E. Tam, S. Xu, and K. Ostrikov, Nanoscale **2**(4), 594–600 (2010).
[39]B. P. Veettil, L. Wu, X. Jia, Z. Lin, T. Zhang, T. Yang, C. Johnson, D. McCamey, G. Conibeer, and I. Perez-Würfl, Appl. Phys. Lett. **105**(22), 222108 (2014).
[40]X. J. Hao, E. C. Cho, G. Scardera, E. Bellet-Amalric, D. Bellet, Y. S. Shen, S. Huang, Y. D. Huang, G. Conibeer, and M. A. Green, Thin Solid Films **517**(19), 5646–5652 (2009).
[41]X. J. Hao, E. C. Cho, C. Flynn, Y. S. Shen, G. Conibeer, and M. A. Green, Nanotechnology **19**(42), 424019 (2008).
[42]J. Müller, B. Rech, J. Springer, and M. Vanecek, Sol. Energy **77**(6), 917–930 (2004).
[43]Z. Lin, I. Perez-Wurfl, L. Wu, X. Jia, T. Zhang, B. Puthen-Veettil, H. Zhang, D. Di, and G. Conibeer, Proc. SPIE **8620**, 86201W (2013).
[44]T. Fricke-Begemann, N. Wang, P. Peretzki, M. Seibt, and J. Ihlemann, J. Appl. Phys. **118**(12), 124308 (2015).